Hyperfine Coupling in Methyl Radical Isotopomers

Iain McKenzie,[†] Jean-Claude Brodovitch, Khashayar Ghandi,[‡] Brett M. McCollum, and Paul W. Percival*

Department of Chemistry and TRIUMF, Simon Fraser University, 8888 University Drive, Burnaby, B.C. V5A 1S6, Canada

Received: June 14, 2007; In Final Form: August 4, 2007

The hyperfine coupling constants (hfcs) of two methyl radical isotopomers, CH_2Mu and CD_2Mu, have been measured over a wide range of temperature in ketene and ketene-d_2, from which the radicals were generated. The magnitudes of the hfcs of these muoniated methyl radical isotopomers are larger than those of CH_3 and CD_3 due to larger zero-point energy in the out-of-plane bending mode. In contrast to CH_3 and CD_3, where the coupling constants become smaller with increasing temperature, the negative hfcs of the muoniated radicals were found to increase in magnitude (become more negative) with temperature, passing through a maximum near the boiling point of ketene. This behavior is attributed to a solvent-induced change in the force constant of the out-of-plane bending mode. The opposite temperature effect known for CH_3 and CD_3 is explained by excitation of the low frequency out-of-plane bending mode. This effect is much smaller in the muoniated radicals, where the vibrational frequency is significantly higher due to the light mass of muonium; consequently, the solvent effect dominates at low temperatures.

1. Introduction

The methyl radical is the simplest organic π-radical and an important intermediate in many reactions in such diverse fields as atmospheric chemistry, combustion, and biochemistry. However, it is very reactive and its short lifetime makes it challenging to study. It was first identified by Herzberg and Shoosmith using flash photolysis and ultraviolet (UV) absorption spectroscopy[1] and subsequently studied by infrared (IR) spectroscopy in several low-temperature matrices[2−4] and in the gas phase.[5−7] The optical spectroscopic studies have shown that the methyl radical is an oblate symmetric top with a planar equilibrium geometry in the ground electronic state ($X\ ^2A_2$). The methyl radical is often considered to be a benchmark for theoretical calculations because its small size allows for extensive calculations that can include vibrational averaging and solvent effects.[8−15] The computational studies predict that the protons have a negative hyperfine constant (hfc). This was confirmed experimentally by Davis et al., who were able to resolve the hyperfine splittings in the IR spectrum of methyl radicals generated with low rotational temperatures (∼25 K).[7]

One of the most useful and versatile techniques for studying free radicals is electron paramagnetic resonance (EPR), which can measure the hfcs and thus provide information about the distribution of unpaired spin density in the radical.[16−18] The configuration and conformation of a radical can be inferred from measurements of the magnitude, sign, and temperature dependence of the hfcs. There have been many EPR experiments on the methyl radical in different matrices and solvents;[19−36] as evident from Table 1, the proton hfc varies with environment and generally decreases with increasing temperature in the liquid phase.

TABLE 1: Isotropic Proton Hyperfine Coupling Constant of the Methyl Radical

environment	*T*/K	$\lvert A_p\rvert$/MHz	ref
vacuum	25	65.5(9)	7
H_2	4	65.07(13)	19
Ar	4	64.64(20)	19
Kr	4	64.46	23
	85	64.46	20
Xe	4	64.37(14)	24
CH_4	4	64.39(18)	19
	96	64.57(3)	20
CO	4	64.55	31
CH_3COCH_3	110	62.78	28
	220	63.98	22
n-hexane	250	64.04(1)[a]	25
CH_3OH	250	64.03(1)[b]	25
1:1 CH_3OH:H_2O	250	63.94(1)[c]	25
H_2O	77	63.06	27
	231	63.65(4)	26
	300	63.53(1)[d]	21

[a] $63.96 - [(3.6(0.6)) \times 10^{-3}\ (T\text{-}273)]$ over the range 220−270 K. [b] $63.93 - [(4.2(0.6)) \times 10^{-3}\ (T\text{-}273)]$ over the range 210−280 K. [c] $63.82 - [(5.0(0.6)) \times 10^{-3}\ (T\text{-}273)]$ over the range 240−280 K. [d] $63.544(8) - [(5.9(0.6)) \times 10^{-3}\ (T\text{-}298)]$ over the range 280−333 K.

Further information about the structure and dynamics of organic radicals can be obtained by studying isotopically substituted molecules. All of the possible deuterated methyl radicals (CH_2D, CHD_2, and CD_3) have been observed by EPR.[20,23] Additional information about the methyl radical could be obtained by studying its muoniated isotopomers: CH_2Mu and CD_2Mu. These are radicals that contain muonium (Mu) as a polarized spin-label. Muonium is a single-electron atom with the positive muon (μ^+) as nucleus and is considered to be a light isotope of hydrogen.[35] Mu can be formed by the implantation of μ^+ into a solid, liquid or gas sample,[38] and muoniated radicals can form by the addition of Mu to an unsaturated bond. The very light mass of the muon ($m_\mu \sim m_p/9$) can have a large effect on the vibrational motion of a radical in which it is present and may possibly lead to the observation of effects that cannot

* Corresponding author. e-mail: percival@sfu.ca.
[†] Present address: ISIS, CLRC Rutherford Appleton Laboratory, Didcot, Oxon OX11 0QX, U.K., and School of Chemical Sciences and Pharmacy, University of East Anglia Norwich, NR4 7TJ, U.K.
[‡] Present address: Department of Chemistry, Mount Allison University, 63C York Street, Sackville, N.B., Canada, E4L 1G8.

10.1021/jp0746190 CCC: $37.00
Published on Web 10/04/2007

SCHEME 1: Formation of the Muoniated Trimethylsilylmethyl Radical

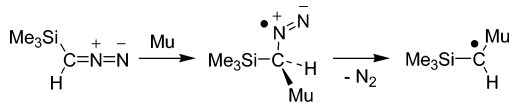

SCHEME 2: Formation of the Muoniated Methyl Radical

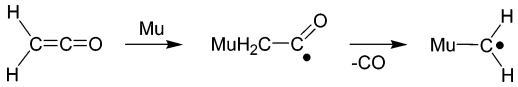

be seen with other isotopes.[39,40] These effects are manifested by changes in the magnitude and temperature dependence of the hfcs. In order to compare the hfcs of different isotopes, which have different gyromagnetic ratios (γ), we will refer to the proton-equivalent reduced hfc, which is denoted by a prime and is given by $A'_X = A_X(\gamma_p/\gamma_X)$.

Beams of monoenergetic muons are available in which the spin polarization is close to 100%. The positive muon is radioactive with a lifetime of 2.2 μs and decays to a positron and two neutrinos: $\mu^+ \rightarrow e^+ + \nu_e + \bar{\nu}_\mu$. During this decay, the positron is emitted preferentially along the direction of the muon's spin; thus the detection of decay positrons in a given direction provides a convenient means of monitoring the spin polarization of an ensemble of muons. The muon and nuclear hfcs of a muoniated radical can be determined using transverse-field muon spin rotation (TF-μSR) and avoided muon level-crossing resonance (μLCR), respectively. These powerful magnetic resonance techniques can be used to study radicals in a wide variety of environments.[41,42]

To date, over 200 muoniated radicals have been studied, almost all of which have Mu attached to an atom that is adjacent (or β) to the radical center (α-carbon). This is a consequence of formation of the radicals by Mu addition to an unsaturated bond. There are only a few examples of radicals where Mu is attached directly to the radical center (the α-position), because they are difficult to produce; however, two routes to generate these radicals have recently been developed.[43] The first route involves addition to an unsaturated bond, followed by rapid decomposition of the β-muoniated radical to give an α-muoniated radical. In order for spin polarization to be transferred to the α-muoniated radical, the decomposition must occur within a few nanoseconds; this can occur when there is a good leaving group like N_2 or CO present, such as in molecules with diazo and ketene functional groups.[44] The other route to generate α-muoniated radicals is by the addition of Mu to stable carbenes.[44]

An early attempt to produce the muoniated methyl radical by the reaction of Mu with diazomethane was unsuccessful,[45] most likely due to the extreme instability of diazomethane at the high concentrations required for TF-μSR experiments (typically 1 M or greater). However, it proved possible to produce a substituted muoniated methyl radical by the reaction of Mu with a more stable diazo compound, trimethylsilyldiazomethane (Scheme 1). From the temperature dependence of the muon hyperfine constant it was deduced that the radical center is nonplanar, and this was ascribed to the influence of the trimethylsilyl group.[46,47]

We have previously reported the successful detection of the CH_2Mu radical produced by the reaction of Mu with ketene at 184 K (Scheme 2).[48] The intermediate muoniated acetyl radical was not observed, nor were any of the radicals that could form by Mu addition to the central carbon or oxygen of ketene. Bennett and Miles studied the reaction of H and D atoms with ketene in water, benzene and adamantane matrices at 77 K using EPR and a rotating cryostat, and found that the major product in H_2O and D_2O matrices was the acetyl radical, of which a considerable portion was found to undergo scission to form the methyl radical.[49]

Information about the structure and dynamics of a radical can be inferred from the information available from μSR or EPR experiments, i.e., the hfcs. However, since the hfcs of a radical depend on both vibrational averaging and solvation, it can be difficult to separate their effects, and it is often valuable to compare the experimental results with *ab initio* calculations. Computational studies can now model the effect of large amplitude motions on the hfcs by calculating the energy and hfcs for a series of fixed geometries and obtaining the vibrational wave function numerically from the ensuing one-dimensional potential.[50] Barone and co-workers have studied the effect of vibrational averaging on the methyl radical and demonstrated that this leads to a decrease in the magnitude of the proton hfc.[12] The effect of vibrational averaging has also been studied for more complex radicals, such as cyclopropyl,[51] glycinyl,[52] and the H atom adducts of cytosine.[53] In this paper we examine the effect of vibrational averaging on the isotopomers of the methyl radical, and also how the vibrationally averaged states are affected by interactions with neighboring molecules.

2. Experimental Methods

2.1. Ketene Synthesis and Sample Preparation. Ketene was produced by the pyrolysis of acetone in a "Hurd" lamp, or ketene generator, using a design based on a description given in Vögel.[54] Acetone was used rather than diketene[55] or acetic anhydride[56] due to the lower cost of the starting material and the ready availability of deuterated samples. The ketene was trapped at 196 K and then purified by vacuum distillation, the middle third fraction being retained. NMR analysis of the sample after the muon experiments revealed the presence of acetone ($\sim$20% mole fraction). The deuterated ketene samples were not analyzed, but since they were prepared in an identical manner it was assumed that there was a comparable amount of deuterated acetone present. The liquid ketene was deoxygenated by the freeze−pump−thaw technique and sealed in a nonmagnetic stainless-steel cell with a 25 μm thick window to allow penetration of the muons. The samples were kept at dry ice temperature until needed, to prevent dimerization of the ketene.

2.2. TF-μSR and μLCR Experiments. The TF-μSR and μLCR experiments were performed over 3 week-long beam periods on the M15 and M20 beamlines at the TRIUMF cyclotron in Vancouver, Canada. Spin-polarized positive muons (4 MeV) were extracted from the beamline and stopped in the sample, which was mounted in the HELIOS μSR spectrometer whose magnetic field was aligned along the beam direction. The spin polarization of the muon beam was perpendicular to the applied magnetic field for the TF-μSR experiments and parallel to the field for μLCR experiments, with the positron counters arranged accordingly. The apparatus and measurement procedures are described in greater detail elsewhere.[39,57]

In the TF-μSR spectrum at high magnetic fields, where the Zeeman energy is much larger than the hyperfine interactions, the radical frequencies form two degenerate groups

$$\nu_R = \nu_D \pm {}^1/_2 A_\mu \qquad (1)$$

where ν_D is the precession frequency of muons in diamagnetic environments (13.55 kHz G^{-1}) and A_μ is the muon hfc.[41] The

TABLE 2: Muon Hyperfine Constants of the CH_2Mu and CD_2Mu Radicals as Determined from TF-μSR Spectra at Different Temperatures[a]

CH_2Mu		CD_2Mu[b]	
T/K	$\lvert A_\mu\rvert$/MHz	T/K	$\lvert A_\mu\rvert$/MHz
73	201.30(10)	81	202.29(5)
88	201.27(7)	93	202.37(2)
109	201.28(3)	105	202.42(2)
131	201.36(4)	113	202.42(2)
152	201.37(4)	125	202.43(2)
173	201.44(6)	137	202.45(3)
184	201.55(4)	140	202.41(3)
205	201.57(7)	150	202.39(4)
212	201.61(6)	160	202.44(4)
223	201.54(8)	170	202.49(4)
		180	202.42(4)
		190	202.51(5)
		200	202.53(5)
		210	202.68(5)
		220	202.66(8)
		225	202.35(7)
		235	202.01(12)

[a] Statistical uncertainties given in parentheses (see text, section 2.2). [b] Two data sets: measurements below 140 K were made with one sample; higher temperature data were obtained with a different sample at a later date.

TABLE 3: μLCR Resonance Fields and the Corresponding Proton Hyperfine Constants of the CH_2Mu Radical at Various Temperatures[a]

T/K	$\lvert A_\mu\rvert$[b]/MHz	B_{res}/G	$\lvert A_p\rvert$/MHz
132	201.34(2)	7489(2)	61.24(5)
152	201.41(2)	7491(2)	61.26(4)
162	201.44(2)	7486(2)	61.39(3)
184	201.51(2)	7485(2)	61.47(3)
192	201.54(2)	7486(3)	61.48(5)
204	201.58(3)	7492(1)	61.42(3)
212	201.61(3)	7491(2)	61.47(4)
223	201.64(3)	7493(3)	61.46(7)

[a] Statistical uncertainties given in parentheses (see text, section 2.2). [b] Linearly interpolated muon hfc values.

magnitude of the muon hfc (in units of frequency) is calculated from the difference in the two precession frequencies.

Resonances in the μLCR spectrum occur at values of the magnetic field where a muon transition frequency is matched to that of some other nucleus in the coupled spin system of a radical. Each magnetic nucleus (characterized by its hyperfine constant, A_k) gives rise to a resonance at a value of the magnetic field determined primarily by the difference between A_μ and A_k:

$$B_{res} = \frac{1}{2}\left[\frac{A_\mu - A_k}{\gamma_\mu - \gamma_k} - \frac{A_\mu^2 - 2MA_k^2}{\gamma_e(A_\mu - A_k)}\right] \quad (2)$$

where M is the z-component of the total spin of the unpaired electron, the muon, and the nucleus involved in the level crossing, and γ_e, γ_μ, and γ_k refer to the gyromagnetic ratios of the electron, muon, and other nucleus, respectively.

Both TF-μSR and μLCR experiments involve counting particles and are subject to Poisson statistics. Spectral parameters are determined by multiparameter fits to primary data (time-domain histograms for TF-μSR and positron asymmetry counts for μLCR).[39,57] The uncertainties quoted in Tables 2−4 derive from one-standard-deviation uncertainties in the relevant fit parameters.

2.3. Computation. Density functional calculations on the methyl radical were performed using the Gaussian 03 package of programs.[58] The geometry of the methyl radical was optimized with the unrestricted B3LYP functional[59] and the 6-311++G(2df,p) basis set, and the harmonic and anharmonic vibrational frequencies of the methyl radical isotopomers were calculated at the same level on the optimized structure. The isotopes were included in the calculations using the ReadIsotope option, with the mass of Mu given as 0.1140 amu. The anharmonic vibrational frequencies could not be calculated for molecules with D_{3h} symmetry so the symmetry was artificially reduced to C_{2v} by increasing one of the C−H bonds by 0.01 pm (an arbitrary small value which serves only to break the symmetry).

TABLE 4: μLCR Resonance Fields and the Corresponding Deuteron Hyperfine Constants of the CD_2Mu Radical at Various Temperatures[a]

T/K	$\lvert A_\mu\rvert$[b]/MHz	B_{res}/G	$\lvert A_d\rvert$/MHz
120	202.32(4)	7438(2)	9.45(6)
140	202.38(3)	7443(6)	9.38(15)
160	202.44(2)	7445(6)	9.38(16)
180	202.50(2)	7438(5)	9.63(13)
200	202.56(3)	7440(4)	9.62(11)

[a] Statistical uncertainties given in parentheses (see text, section 2.2). [b] Linearly interpolated muon hfc values.

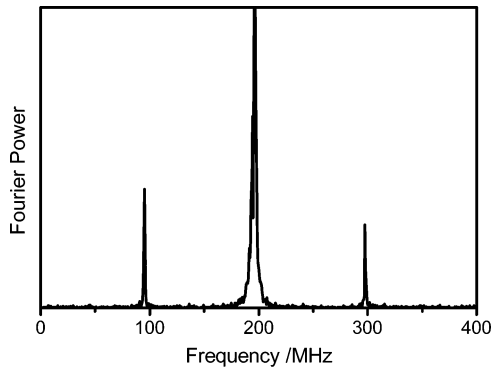

Figure 1. TF-μSR spectrum from deuterated ketene at 180 K in a transverse magnetic field of 14.5 kG. The signal at 196 MHz is due to muons in diamagnetic environments; it has been truncated to better display the pair of peaks at 95 and 298 MHz, which are due to the radical CD_2Mu.

3. Results

3.1. Muon Spin Spectroscopy. When ketene was irradiated with positive muons the TF-μSR spectrum showed only one type of radical, previously identified as the CH_2Mu radical.[48] Similarly, only one type of radical was observed in the TF-μSR spectrum obtained from deuterated ketene. The muon hfc (A_μ) of the latter radical is almost identical to that of CH_2Mu, leading us to conclude that the observed species is the CD_2Mu radical. A representative TF-μSR spectrum of the CD_2Mu radical is shown in Figure 1. The values of A_μ extracted from such spectra for CH_2Mu and CD_2Mu at different temperatures are listed in Table 2. Separate measurements were made with two deuterated ketene samples, and there is a small discrepancy between the two data sets, which we attribute to different amounts of acetone impurity.

The μLCR spectra of CH_2Mu and CD_2Mu each display only a single resonance. The field positions of these proton and deuteron resonances are almost identical because the change in gyromagnetic ratio for the two nuclei cancels top and bottom in the leading term on the right-hand side of eq 2. However, as is evident from Figure 2, the deuteron resonance in CD_2Mu is much less intense than the proton resonance in CH_2Mu. This is

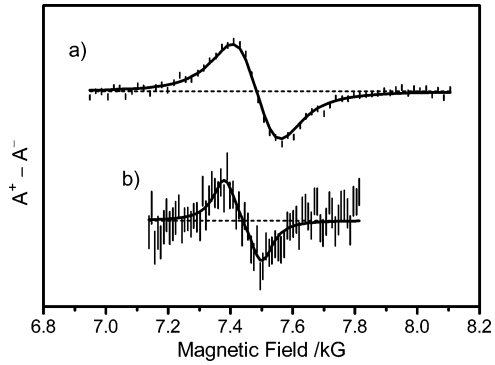

Figure 2. (a) μLCR spectrum of CH_2Mu in ketene at 184 K. b) μLCR spectrum of CD_2Mu in ketene-d_2 at 200 K. The amplitude scale for this resonance has been magnified by a factor of 6.8 to account for the different magnetic moments of the proton and deuteron.

TABLE 5: Computed Energy,[a] Proton Hyperfine Constant, Dipole Moment and Isotropic Polarizability at Fixed Out-of-Plane Angles θ[b] for CH_3

θ/deg	ΔE/kJ mol^{-1}	A_p/MHz	μ/Debye	$\alpha'/10^{-30}$ m^3
0.00	0	−59.71	0	2.0844
3.33	0.504	−57.92	0.1369	2.0842
6.66	2.177	−52.81	0.2674	2.0836
10.00	5.473	−45.01	0.3865	2.0821
13.33	11.064	−35.43	0.4911	2.0797
16.66	19.762	−25.04	0.5806	2.0764
20.00	32.426	−14.69	0.6561	2.0727

[a] UB3LYP/6-311++G(2df,p). [b] θ is defined as the angle between a C−H bond and the plane containing the three H atoms.

because the signal amplitude is proportional to the nuclear gyromagnetic ratio, which is smaller for the deuteron. Resonance fields and corresponding hfcs at different temperatures are reported in Tables 3 and 4. The field positions indicate that the muon, proton and deuteron hfcs have the same sign.

Apart from the small changes in values reported in the tables, there was no change in either type of spectrum until the sample was heated above 220 K, when a second radical with a larger muon hfc was observed in the TF-μSR spectrum and the intensity of the methyl radical signals were greatly diminished. The methyl radical signals disappeared entirely by 235 K. The new signals can readily be assigned to the Mu adduct of diketene (addition to the terminal carbon of the C=C bond), based on the magnitude and temperature dependence of the muon hfc as determined previously in a separate study using pure diketene.[60]

3.2. Computation. The optimized structure of the methyl radical was calculated to have D_{3h} symmetry with a C−H bond length of 1.0795 Å, which is in good agreement with the experimental value of 1.079 Å.[61] The energy, proton hfc, dipole moment (μ), and isotropic polarizability (α) of CH_3 were calculated as a function of the out-of-plane angle θ and are listed in Table 5.

The harmonic vibrational frequencies for CH_3, CH_2Mu, and CD_2Mu calculated at the UB3LYP/6-311++G(2df,p) level are listed in Table 6. The results for CH_3 are in good agreement with experimental and calculated values reported in the literature.[61] Although the out-of-plane bending potential is better described by a quartic function, a harmonic potential reproduces the calculated values well (Figure 3). The anharmonic vibrational frequencies were also calculated with Gaussian03, and were found to be lower than the harmonic frequencies except for the out-of-plane bending mode. In the latter case the quartic potential is approximated by an extended harmonic curve when a large section of the potential surface is examined. Throughout this paper we have made the approximation that the out-of-plane bending potential is harmonic. This facilitates the development of analytical expressions to describe the temperature dependence of the hfcs, rather than a more rigorous but less descriptive approach using higher-order functions and numerical solution. It is clear that the light mass of the muon has a large effect on the vibrational frequencies, especially for the out-of-plane mode and the in-plane stretching frequencies involving Mu.

4. Discussion

4.1. Magnitude of the Hyperfine Coupling Constants. Although magnetic resonance techniques typically only provide the magnitude (and not the sign) of the hyperfine constant from splittings in the frequency spectrum, computational and optical spectroscopic studies have conclusively demonstrated that the proton hfc of the methyl radical is negative. This can be explained by a delicate balance between two effects: spin polarization of the C−H bond,[62] which contributes negative spin density, and direct overlap with the singly occupied molecular orbital (SOMO), which contributes positive spin density. The negative sign of the hfc indicates that spin polarization dominates, but the balance of effects means that the proton hfc is very sensitive to the configuration at the radical center.[11,12,14] Out-of-plane bending brings the substituents out of the nodal plane of the SOMO, increasing the positive contribution of spin density and resulting in a smaller magnitude (less negative) coupling constant. Temperature dependence arises primarily through excitation of the low frequency out-of-plane vibrational mode. For the following discussion it is sufficient to treat this mode as harmonic (a reasonable approximation according to Figure 3).

The vibrationally averaged hfc in a given vibrational state is given by the expectation value

$$A'_X{}^{(v)} = \langle \psi_v(s) | A'_X(s) | \psi_v(s) \rangle \qquad (3)$$

where $\psi_v(s)$ is the normalized harmonic wave function for vibrational level v, and $A'_X(s)$ is the dependence of the hfc of nucleus X on the displacement coordinate s (defined here as $R(\theta_1 + \theta_2 + \theta_3)/\sqrt{3}$, where R is the C−H bond length and the θ_is refer to the angles between each C−H bond and the plane formed by the hydrogen atoms). Vibrational states above the ground level include greater weighting from nonplanar configurations, so these hfcs are less negative than in the ground state.

The hfc at a given temperature corresponds to the Boltzmann weighted average over all the vibrational levels. However, the out-of-plane bending frequency of CH_3 ($\bar{\nu}$ = 606 cm^{-1}) is sufficiently high that only the ground and first excited vibrational levels need to be considered in modeling the temperature dependence below room temperature. Thus

$$A'_X(T) = \frac{A'_X{}^{(0)} + A'_X{}^{(1)} e^{-hc\bar{\nu}/kT}}{1 + e^{-hc\bar{\nu}/kT}} \qquad (4)$$

Except at very low temperature (discussed later), the hfcs for CH_3, CH_2D, CHD_2 and CD_3 all decrease with increasing temperature, consistent with increasing population of the ν = 1 level, whose wave function has a node at $\theta = 0°$ (i.e., planar geometry). Small differences in the temperature dependence arise from the different out-of-plane vibrational frequencies, as predicted by eq 4. In contrast, the population of the $\nu = 1$ level in the muoniated isotopomers can be shown to be negligible, even up to room temperature, due to the much higher out-of-plane bending frequencies. The proton hfcs in the $v = 0$ and $v = 1$ levels can be estimated from the temperature dependence of the proton hfc in solution.[25] Using these values (scaled for

TABLE 6: Calculated Harmonic Vibrational Modes for CH_3, CH_2Mu, and CD_2Mu[a]

	CH_3		CH_2Mu		CD_2Mu	
mode	$\bar{\nu}$/cm^{-1}	$\bar{\nu}$/cm^{-1} (lit.)[b]	mode	$\bar{\nu}$/cm^{-1}	mode	$\bar{\nu}$/cm^{-1}
out-of-plane bend	539	606	out-of-plane bend	945	out-of-plane bend	903
symmetric in-plane bend (degenerate)	1407	1396	symmetric in-plane bend	1410	symmetric in-plane bend	1046
			symmetric C−H stretch	3167	symmetric C−D stretch	2283
symmetric C−H stretch	3108	3004	asymmetric C−H stretch + C-Mu wag	3247	asymmetric C−D stretch	2447
asymmetric C−H stretch (degenerate)	3284	3161	asymmetric C−H stretch + C-Mu wag	3398	C-Mu wag	3316
			C-Mu stretch	9272	C-Mu stretch	9273

[a] UB3LYP/6-311++G(2df,p)//UB3LYP/6-311++G(2df,p) using Gaussian 03. [b] Experimental data from ref 61

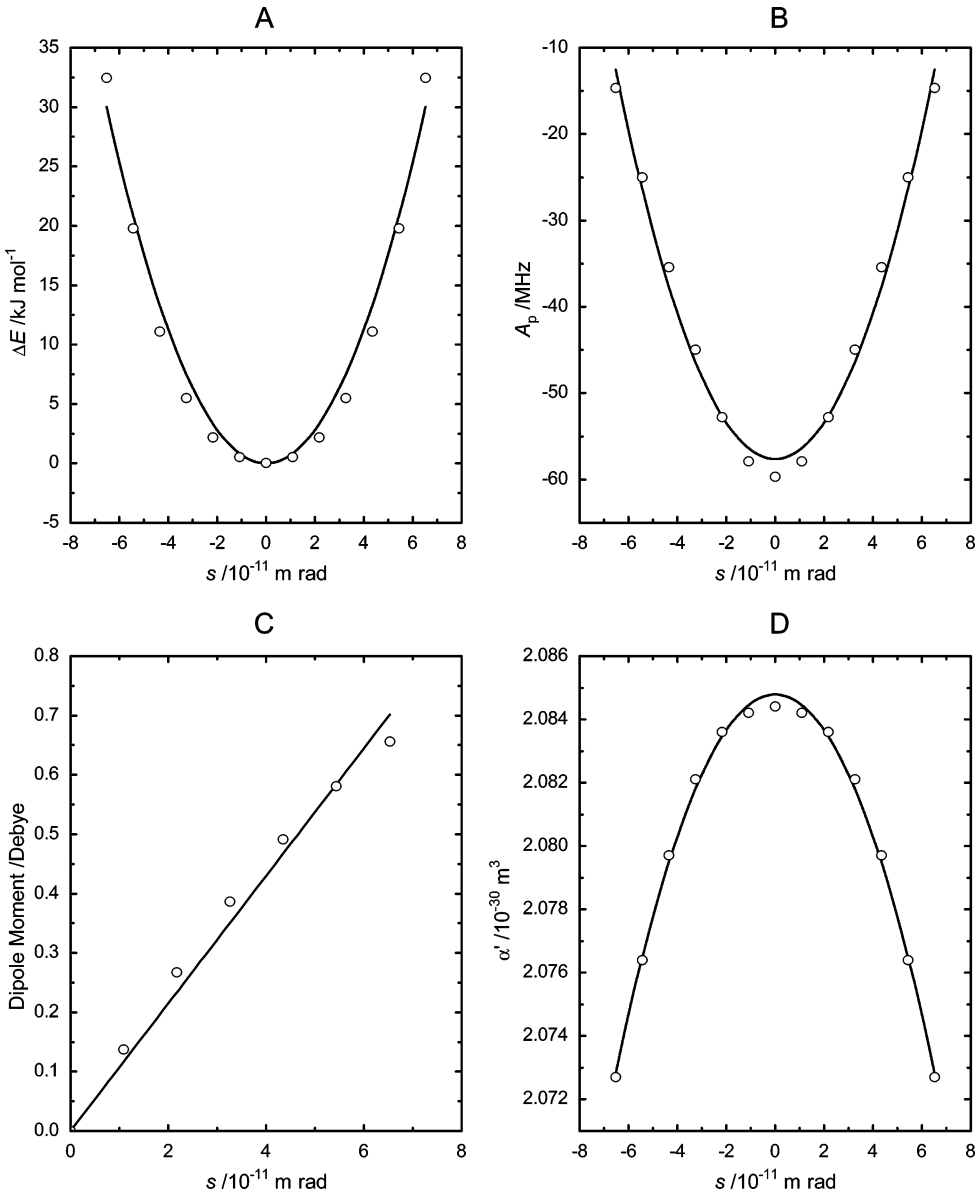

Figure 3. Computed (UB3LYP/6-311++G(2df,p) level) dependence of various methyl radical properties on the out-of-plane displacement *s*: (A) energy; (B) proton hyperfine coupling constant; (C) dipole moment; (D) isotropic polarizability volume.

the muon gyromagnetic ratio), and the calculated out-of-plane bending frequency, we estimate that the change in the muon hfc between 100 and 225 K for CH_2Mu and CD_2Mu should be less than 0.01 MHz from this effect. Thus, a study of the muoniated isotopomers can reveal contributions to the temperature dependence of hfcs which might otherwise be obscured by dominant vibrational effects in the non-muoniated radicals.

The hfcs of CH_2Mu and CD_2Mu are significantly different from both the non-muoniated isotopomers and from each other. These differences are larger than the predicted solvent effects, which are of the order of 1 MHz (see later), and must be ascribed to intramolecular effects. Indeed, Fessenden noted that there are significant differences in the hfcs of the H/D isotopomers of the methyl radical, even when they are in similar chemical environments, and suggested that the differences arise from the amount of averaging in the ground vibrational state of the out-of-plane mode.[23] The strong angular dependence of the hfcs means that their averaged values are very sensitive to the shape of the vibrational wave function, which is dependent on the mass of the atoms. The ground state vibrational wave function for the out-of-plane mode is more localized for heavier isotopomers, such as CD_3, than for lighter isotopomers such as

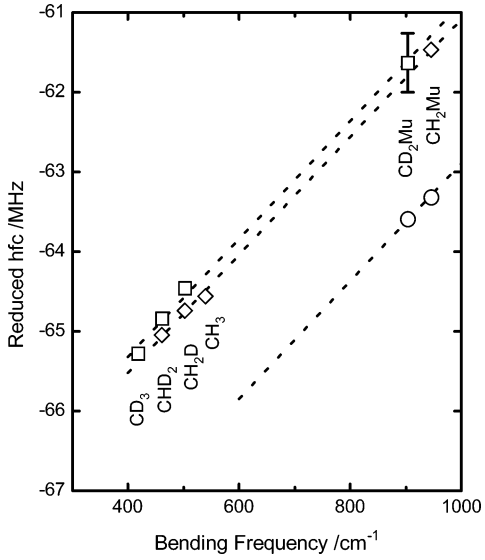

Figure 4. Reduced hyperfine coupling constants of the muon (○), proton (◇), and deuteron (□) plotted vs the calculated harmonic out-of-plane bending frequencies (UB3LYP/6-311G(2df,p)) for methyl radical isotopomers under the stated conditions: CD_3 (methane, 96 K), CHD_2 (krypton, 86 K), CH_2D (krypton, 86 K), CH_3 (methane, 96 K), CD_2Mu (liquid ketene-d_2; Mu hfc at 180 K, D hfc averaged over liquid range) and CH_2Mu (liquid ketene, 184 K). The dotted lines depict a fit to eq 7 (see text).

CH_2Mu, due to the differences in the zero-point energy. Thus, the CH_2Mu isotopomer has a larger contribution from nonplanar configurations than CD_3, which results in the averaged hfcs for CH_2Mu being smaller than the averaged hfcs in CD_3. The computational data displayed in Figure 3B show that to a very good approximation the proton hfc has a quadratic dependence on the out-of-plane displacement, so that the reduced hfc for various isotopes X can be expressed by

$$A'_X(s) = f_X A_0 + A_2 s^2 \tag{5}$$

where A_0 is negative, A_2 is positive, and the factor f_X accounts for the isotope effect, which arises from vibrational averaging of the anharmonic bond-stretching mode.[63]

The vibrationally averaged reduced proton hfc is obtained by substituting eq 5 into eq 3, giving

$$A'^{(0)}_X = f_X A_0 + \frac{A_2 \hbar}{2 m_r^{1/2} k_s^{1/2}} \tag{6}$$

where m_r is the reduced mass and k_s is the force constant of the out-of-plane bending mode.

This equation can be rewritten in terms of the harmonic out-of-plane vibrational frequency ($\bar{\nu}^H$) to give:

$$A'^{(0)}_X = f_X A_0 + \frac{A_2 hc}{2k_s} \bar{\nu}^H \tag{7}$$

This predicts that $A'^{(0)}_X$ should be linearly dependent on $\bar{\nu}^H$. The reduced hfcs of methyl isotopomers at low temperature (where most of the molecules are in the $\nu = 0$ state) are plotted vs the calculated harmonic out-of-plane frequency in Figure 4. The dotted lines correspond to a fit to eq 7, with a common slope (7.4×10^{-3} MHz/cm^{-1}) but different isotope factors f_X (0.997 for D, 1.000 for H, and 1.026 for Mu). This empirical slope is in good agreement with the value (9.0×10^{-3} MHz/cm^{-1}) determined by evaluating the factor ($^1/_2 A_2 hc/k_s$), considering the approximations employed in the derivation of eq 7.

4.2. Solvent Effects on the Hyperfine Coupling Constants. Unlike the non-muoniated methyl radical isotopomers, the magnitudes of the muon and proton hfcs of CH_2Mu increase with temperature in liquid ketene. This is also the case for the muon hfc of CD_2Mu, but given the large uncertainty in the deuteron hfcs it is not possible to characterize their temperature dependence. For both muoniated isotopomers there is a maximum in $|A_\mu|$ close to the boiling point of ketene (bp 217 K), which suggests an environmental effect.

The proton and ^{13}C hfcs of the methyl radical both depend on the solvent.[25,29] The nature of the solvent can influence the hfcs of solute radicals in two ways—by causing small changes in the structure of the radical or by modification of the interactions between the radical and the solvent. The latter effect operates via transfer of unpaired spin density, so it is not surprising to find that hyperfine constants often correlate with solvent parameters such as dielectric constant, density, or hydrogen-bonding ability. For example, the ^{14}N hfcs of nitroxide radicals have been found to depend on solvent polarity: there is a linear correlation with $(\epsilon\text{-}1)/(\epsilon+2)$, where ϵ is the dielectric constant of the solvent.[64,65] Such an effect has been explored by Fernandez et al.[66] by applying a multiconfiguration self-consistent field method to calculate hfc values for methyl radicals embedded in spherical voids in various solvents. They found a correlation between the shift of the hfc from the vacuum value and the dielectric constant of the solvent. Their data are consistent with the relation

$$\Delta A = A_p^{vac} - A_p(\epsilon) = -0.312\left(\frac{\epsilon - 1}{\epsilon + 2}\right) \tag{8}$$

Since the dielectric constants of typical solvents decrease with temperature, eq 8 suggests that there will be an increase in magnitude of the hyperfine constant with increase in temperature. This is in qualitative accord with our observations. However, the observed change in the reduced muon hfc over the liquid range of ketene is 0.1 MHz, and although we do not know the dielectric constant of ketene, it would have to change by a physically unrealistic amount to account for the ~30% change in the function $(\epsilon - 1)/(\epsilon + 2)$ required to reproduce our results. We conclude that the change of the dielectric constant with temperature contributes only part of the observed temperature dependence of A_μ.

The proton hfc of the methyl radical has been found to vary with the nature of inert matrices at 4 K. There have been several *ab initio* studies of the interaction of the methyl radical with diamagnetic molecules, such as CH_4,[67] HCCH,[68] HCN,[69] HF,[68,70] and H_2O,[71] and in all of these studies the minimum energy geometry of the methyl radical was found to be slightly nonplanar. The interaction with the solvent causes the out-of-plane bending potential of CH_3 to resemble that of CH_2F, resulting in the ground state wave function having a lower amplitude for $\theta = 0$ and the averaged hfc being lower than the gas-phase value, just as the proton hfc of CH_2F is lower than that of CH_3.[12] It is not reasonable to suggest that this will occur in inert matrices or in solution where the radical is completely surrounded by neighboring molecules as the symmetric environment would result in the average minimum being at $\theta = 0°$. The *ab initio* calculations of Takada and Tachikawa demonstrate that the observed dependence on the matrix is not simply due to transfer of spin polarization onto matrix atoms. They calculated the proton hfc of a planar methyl radical in several model matrices ($CH_3(H_2)_n$ (n = 12 and 20), $CH_3(Ar)_n$ (n = 12 and 18), and $CH_3(CH_4)_n$ (n = 12 and 18)) and found that the

magnitude of the proton hfc in the inert matrices is larger than in the gas phase.[72]

Davis et al.[7] noticed that the proton hfc is correlated with the enthalpy of vaporization of the matrix (ΔH_{vap}), which they considered to be related to the strength of the interaction between CH_3 and the matrix molecules. Davis et al.[7] and Stratt and Desjardins[73] speculated that the dependence of A_p on the matrix could be due to the neighboring molecules stabilizing nonplanar configurations of the umbrella bend coordinate. The advantage of using ΔH_{vap} to describe the interaction between the methyl radical and the surrounding molecules is that it is a bulk property that is known for many materials. On the other hand, it gives no insight into the nature of the interaction between the solute and the matrix.

An alternative approach, which we have followed, is to consider the interaction energy between CH_3 and the neighboring atoms or molecules (E_{R-N}), which is the sum of the induced dipole−induced dipole (or dispersion) interaction energy and the dipole−induced dipole interaction energy, and to consider what effect E_{R-N} has on the bending potential of the methyl radical.

$$E_{R-N} = -\frac{3}{2}\frac{\alpha'_{CH_3}(s)\alpha'_N}{d^6}\left(\frac{I_{CH_3}I_N}{I_{CH_3}+I_N}\right) - \frac{\alpha'_{CH_3}(s)\mu_N{}^2}{4\pi\epsilon_0 d^6} - \frac{\alpha'_N\mu_{CH_3}{}^2(s)}{4\pi\epsilon_0 d^6} \quad (9)$$

where α'_{CH_3} and α'_N are the polarizability volumes of the methyl radical and the matrix, respectively, I_{CH_3} and I_N are their ionization energies, μ_{CH_3} and μ_N are their dipole moments, d is the distance between the methyl radical and the neighboring molecules, and ϵ_0 is the permittivity of free space. The dipole−dipole interaction is not included in eq 9 because methyl has no permanent dipole, and dipolar interactions involving nonplanar configurations are averaged to zero by a rate of methyl inversion which is faster than orientation of solvent dipoles. The d^{-6} dependence of E_{R-N} means that in practice we need only consider the molecules that are nearest neighbors to the methyl radical. The matrices in which the methyl radical was studied at 4 K have face centered cubic or hexagonal close packed structures and the methyl radical occupies a substitutional site, which means that in all cases the methyl radical is surrounded by 12 equivalent neighbors. The distance between the methyl radical and the neighboring matrix molecules was set as the sum of effective radii, as determined from the appropriate crystallographic lattice constants. The vdW radius and polarizability volume of the methyl radical are not known but are assumed to be the same as for methane.

Our DFT calculations show (Figure 3D) that the polarizability of CH_3 has a quadratic dependence on the out-of-plane displacement

$$\alpha'_{CH_3}(s) \approx \alpha'_0 - \alpha'_2 s^2 \quad (10)$$

Similarly, the calculations show (Figure 3C) that the dipole moment is roughly proportional to s:

$$\mu_{CH_3}(s) \approx \mu_1 s \quad (11)$$

Expanding (9) using (10) and (11) gives

$$E_{R-N} = -\frac{3}{2}\frac{\alpha'_0\alpha'_N}{d^6}\left(\frac{I_{CH_3}I_N}{I_{CH_3}+I_N}\right) + \frac{3}{2}\frac{\alpha'_2\alpha'_N}{d^6}\left(\frac{I_{CH_3}I_N}{I_{CH_3}+I_N}\right)s^2 - \frac{\alpha'_N\mu_1{}^2}{4\pi\epsilon d^6}s^2 - \frac{\alpha'_0\mu_N{}^2}{4\pi\epsilon_0 d^6} + \frac{\alpha'_2\mu_N{}^2}{4\pi\epsilon_0 d^6}s^2 \quad (12)$$

However, since we are interested in how E_{R-N} varies with s, only terms that depend on s need to be retained; the others merely shift the energy of the radical by a fixed amount. Furthermore, the final term can be neglected as it is much smaller than the others.

The energy of the distorted structures including the interaction energy with neighboring molecules is given by

$$E(s) = \frac{1}{2}k_s s^2 + \sum_n E_{R-N} \quad (13)$$

where the summation need only be taken over nearest-neighbor molecules because E_{R-N} falls with distance to the sixth power. Thus

$$\Delta E(s) = \frac{1}{2}k_s s^2 - \frac{1}{2}\left[\left[\frac{\mu_1{}^2}{2\pi\epsilon_0} - 3\alpha'_2\left(\frac{I_{CH_3}I_N}{I_{CH_3}+I_N}\right)\right]\frac{n\alpha'_N}{d^6}\right]s^2 \quad (14)$$

The preceding equation can be used to define a new force constant for the out-of-plane bending motion in condensed environments

$$k'_s = k_s - \left[\frac{\mu_1{}^2}{2\pi\epsilon_0} - 3\alpha'_2\left(\frac{I_{CH_3}I_N}{I_{CH_3}+I_N}\right)\right]\frac{n\alpha'_N}{d^6} \quad (15)$$

where n is the number of surrounding atoms or molecules.

Combining eqs 6 and 15, and assuming that the modification to the bending potential is small so that the approximation $(1 - x)^{-1/2} \approx 1 + {}^1/_2x$ for $x \ll 1$ is applicable, results in

$$A'^{(0)}_X = A'^{(0),gas}_X + \frac{1}{2}K\frac{n\alpha'_N}{d^6} \quad (16)$$

where $A'^{(0),gas}_X$ is the averaged reduced proton hfc of the $\nu = 0$ level in the absence of interactions with neighboring species and is given by eq 6. The factor K, which is given by

$$K = \frac{A_2\hbar}{2m_r{}^{1/2}k_s{}^{1/2}}\left[\frac{\mu_1{}^2}{2\pi\epsilon_0 k_s} - \frac{3\alpha'_2}{k_s}\left(\frac{I_{CH_3}I_N}{I_{CH_3}+I_N}\right)\right] \quad (17)$$

is not very sensitive to the nature of the matrix, since the second term in the square brackets is significantly smaller than the first and the ionization energies of the inert matrices are very similar to each other and larger than that of the methyl radical.

Equation 16 predicts a linear relationship between the proton hfcs at 4 K in inert matrices and $n\alpha'_N/d^6$, which is confirmed by Figure 5. It can be shown that E_{R-N} and the enthalpy of vaporization, ΔH_{vap}, both depend linearly on $n\alpha'_N/d^6$, so we can write

$$A'^{(0)}_X = A'^{(0),gas}_X + \frac{1}{2}\Phi|E_{R-N}| \approx (A'^{(0),gas}_X + C') + \frac{1}{2}\Gamma\Delta H_{vap} \quad (18)$$

where C' is a constant, which agrees with the observation of Davis et al.

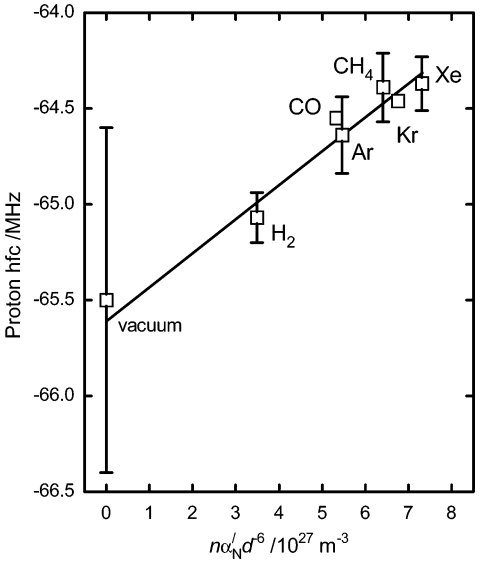

Figure 5. Variation of the proton hyperfine coupling constant of the methyl radical in inert matrices at 4 K with $n\alpha'_N d^{-6}$ (see eq 16 in the text).

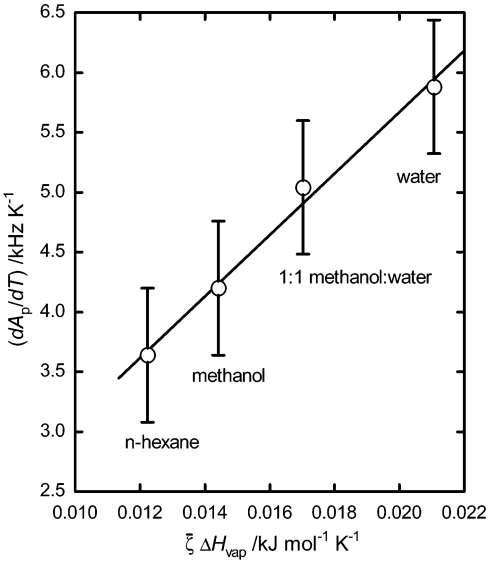

Figure 6. Variation of the temperature dependence of the proton hyperfine coupling constant of the methyl radical in solution[25] with the enthalpy of vaporization[74] of the solvent at 25 °C (eq 21 in the text).

The temperature dependence of the proton hfc of the methyl radical in solution depends on the solvent.[21,25] This effect can also be explained by solvent-mediated changes in the bending potential. Since the temperature dependence arises from population of the first excited vibrational state of the out-of-plane mode, it is necessary to consider what effect changing the bending potential has on the averaged hfc of this level. Following the same procedure used for the ground vibrational state, we can show that the dependence of $A'_X{}^{(1)}$ on the radical-neighbor interaction energy is three times that of $A'_X{}^{(0)}$.

$$A'_X{}^{(1)} = A'_X{}^{(1),\mathrm{gas}} + \frac{3}{2}\Phi|E_{\mathrm{R-N}}| \approx (A'_X{}^{(1),\mathrm{gas}} + C'') + \frac{3}{2}\Gamma\Delta H_{\mathrm{vap}} \tag{19}$$

The temperature dependence of the reduced proton hfc is obtained by differentiating eq 4 with respect to temperature, followed by substitution of eqs 18 and 19 to give

$$\frac{dA'_X(T)}{dT} \propto \left[\frac{\mathrm{e}^{-h\nu/kT}}{(1+\mathrm{e}^{-h\nu/kT})^2}\frac{h\nu}{kT^2}\right]\Gamma\Delta H_{\mathrm{vap}} \tag{20}$$

Other researchers have assumed that the temperature dependence of the proton hfc of CH_3 in solution is linear over a small temperature range.[21,25] We have therefore evaluated the average value of the term in the square bracket over the temperature range of the EPR experiments, $\bar{\xi}$, and rewritten eq 20 as

$$\frac{dA'_X(T)}{dT} \propto \Gamma(\bar{\xi}\Delta H_{\mathrm{vap}}) \tag{21}$$

It is immediately apparent from Figure 6 that the temperature dependence of the proton hfc in solution is linearly dependent on $\bar{\xi}\Delta H_{\mathrm{vap}}$, and we can therefore conclude that the variation in the temperature dependence of A_p for CH_3 in solution is consistent with modification of the out-of-plane bending force constant.

From the slope of Figure 6 we deduce that Γ for A_p in solution is 0.262(13) MHz mol kJ^{-1}. An equivalent parameter can be obtained from the variation of A_p for methyl in the inert matrices at 4 K. In this case Γ is found to be 0.127(23) MHz mol kJ^{-1}. which is within a factor of 2 of the value found for solution. Given the different environments and the approximations involved in the derivation of eq 21, we consider this reasonable agreement.

The temperature dependence of the hfcs in the muoniated methyl radicals is due to changes in the average distance between the methyl radical and the surrounding ketene molecules. The sample cells were not completely full so the ketene could expand with increasing temperature. The distance between the methyl radical and the surrounding ketene molecules is not known experimentally but we have assumed that it is proportional to the inverse cube root of the density of ketene ($\rho_{\mathrm{ketene}}{}^{-1/3}$). Then if eq 16 is rewritten in terms of a new constant (Θ_{ketene}) that describes the methyl radical−ketene interaction, we find that the reduced hfc depends on the square of ketene's density:

$$A'_X = A'_X{}^{(0),\mathrm{gas}} + \Theta_{\mathrm{ketene}}\rho_{\mathrm{ketene}}{}^2 \tag{22}$$

The density of ketene decreases with increasing temperature, and $\rho_{\mathrm{ketene}}{}^2$ is approximately proportional to temperature over the range studied in these experiments.[75] Thus, $\rho_{\mathrm{ketene}}{}^2$ can be approximated by $a - bT$, where $a = 1.159 \times 10^6$ kg^2 m^{-6} and $b = 2.368 \times 10^3$ kg^2 m^{-6} K^{-1}, giving

$$|A'_X| = |A'_X{}^{(0),\mathrm{gas}}| - \Theta_{\mathrm{ketene}}a + \Theta_{\mathrm{ketene}}bT \tag{23}$$

Alteration of the out-of-plane bending force constant of the methyl radical by neighboring molecules will cause the magnitude of the hfcs to increase linearly with temperature, which is in general agreement with the experimental results (Figure 7). Fits of eq 23 to the muon hfcs of CH_2Mu and CD_2Mu in the liquid range give the results shown in Table 7. Deviations from linearity of the experimental data can be attributed to other effects, such as changes in the dielectric constant of ketene with temperature.

The temperature dependence of A_μ is very similar for CH_2Mu and CD_2Mu, which is not surprising given that the measurements were performed in almost identical solvents. The sharp drop in the magnitude of the muon hfcs near the boiling point of ketene is ascribed to changes in the composition of the

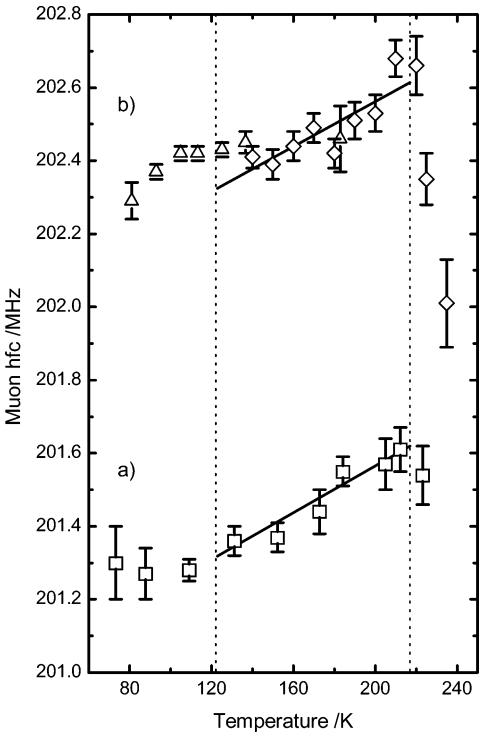

Figure 7. Temperature dependence of the muon hfc in a) CH_2Mu (□) and (b) CD_2Mu (Δ = deuteroketene sample 1; ◇ = deuteroketene sample 2). The vertical dotted lines denote the melting and boiling points of ketene. The solid lines represent the best fits of eq 23 to the data over the liquid range of ketene.

TABLE 7: Gas-Phase Muon Hyperfine Constants and Radical-Ketene Interaction Constants for CH_2Mu and CD_2Mu

radical	Θ_{ketene}/MHz m^6 kg^{-2}	$\lvert A_\mu^{(0),gas}\rvert$/MHz
CH_2Mu	$4.23(15) \times 10^{-7}$	202.49(7)
CD_2Mu	$4.08(13) \times 10^{-7}$	203.45(6)

sample due to the formation of diketene, which is significantly more dense than ketene.

The above analysis shows that the linear dependence of the muon hfc on temperature is consistent with the change in density of the solvent. An alternative approach is to consider the heat of vaporization. For ketene ΔH_{vap} varies linearly with temperature,[75] according to $\Delta\Delta H_{vap}/\Delta T = -0.013$ kJ mol^{-1} K^{-1}. Combining this with eq 18, we predict that the rate of change of A_μ with temperature should be 5.4×10^{-3} MHz K^{-1}, which is similar to the observed values of $3.4(6)\times10^{-3}$ MHz K^{-1} for CH_2Mu and $3.0(7) \times 10^{-3}$ MHz K^{-1} for CD_2Mu.

5. Summary

CH_2Mu and CD_2Mu were produced by the reaction of muonium with ketene and deuterated ketene, respectively. The magnitude of the hfcs in CH_2Mu and CD_2Mu are larger than those of the non-muoniated isotopomers because the larger zero-point energy in the out-of-plane bending mode leads to greater sampling of regions with positive spin density. The temperature dependencies of the muon, proton and deuteron hfcs in these radicals are unlike that of the other methyl radical isotopomers because the larger out-of-plane bending frequency prevents significant population of the excited vibrational level. The interactions with neighboring molecules modify the force constant of the out-of-plane bending mode and the amount of vibrational averaging, and this can account for the variation of $A_p(CH_3)$ in inert matrices at 4 K, the temperature dependence of $A_p(CH_3)$ in solutions near room temperature, and the temperature dependence of the hfcs of CH_2Mu and CD_2Mu in liquid ketene.

Acknowledgment. We thank Dr. Brenda Addison-Jones and Sonja Kecman for assistance with data taking and the staff of the TRIUMF Centre for Molecular and Materials Science for technical support. This research was financially supported by the Natural Sciences and Engineering Research Council of Canada (NSERC) and, through TRIUMF, by the National Research Council of Canada (NRC).

Supporting Information Available: Text giving the complete ref 58 and table giving the output from Gaussian 03 calculations, such as geometry optimization for CH_3; frequency calculations for CH_3, CH_2Mu, CD_2Mu, CD_3, CH_2D, CHD_2, and partial geometry optimization of CH_3 as a function of out-of-plane angle. This material is available free of charge via the Internet at http://pubs.acs.org.

References and Notes

(1) Herzberg, G.; Shoosmith, J. *Can. J. Phys.* **1956**, *34*, 523−525.
(2) Milligan, D. E.; Jacox, M. E. *J. Chem. Phys.* **1967**, *47*, 5146−5156.
(3) Snelson, A. *J. Phys. Chem.* **1970**, *74*, 537−544.
(4) Pacansky, J.; Bargon, J. *J. Am. Chem. Soc.* **1975**, *97*, 6896−6897.
(5) Tan, L. Y.; Winer, A. M.; Pimentel, G. C. *J. Chem. Phys.* **1972**, *57*, 4028−4037.
(6) Yamada, C.; Hirota, E.; Kawaguchi, K. *J. Chem. Phys.* **1981**, *75*, 5256−5264.
(7) Davis, S.; Anderson, D. T.; Duxbury, G.; Nesbitt, D. J. *J. Chem, Phys.* **1997**, *107*, 5661−5675.
(8) Schrader, D. M.; Karplus, M. *J. Chem. Phys.* **1964**, *40*, 1593−1601.
(9) Ohta, K.; Nakatsuji, H.; Maeda, I.; Yonezawa, T. *Chem. Phys.* **1982**, *67*, 49−58.
(10) Botschwina, P.; Flesch, J.; Meyer, W. *Chem. Phys.* **1983**, *74*, 321−338.
(11) Chipman, D. M. *J. Chem. Phys.* **1983**, *78*, 3112−3132.
(12) Barone, V.; Grand, A.; Minichino, C.; Subra, R. *J. Chem. Phys.* **1993**, *99*, 6787−6798.
(13) Bickelhaupt, F. M.; Ziegler, T.; Schleyer, P.; von, R. *Organometallics* **1996**, *15*, 1477−1487.
(14) Tachikawa, H.; Igarashi, M.; Ishibashi, T. *Chem. Phys. Lett.* **2002**, *352*, 113−119.
(15) Al Derzi, A. R.; Fau, S.; Bartlett, R. J. *J. Phys. Chem. A* **2003**, *107*, 6656−6667.
(16) Kochi, J. K. In *Advances in Free Radical Chemistry*; Williams, G. H., Ed.; Academic Press: New York, 1975; Volume 5, pp 189−316.
(17) Weil, J. A.; Bolton, J. R.; Wertz, J. E. *Electron Paramagnetic Resonance*; John Wiley & Sons: New York, 1994.
(18) Atherton, N. M. *Principles of Electron Spin Resonance*; Ellis Horwood Prentice Hall: New York, 1993.
(19) Jen, C. K.; Foner, S. N.; Cochran, E. L.; Bowers, V. A. *Phys. Rev.* **1958**, *112*, 1169−1182.
(20) Fessenden, R. W.; Schuler, R. H. *J. Chem. Phys.* **1963**, *39*, 2147−2195.
(21) Zlochower, I. A.; Miller, W. R., Jr.; Fraenkel, G. K. *J. Chem. Phys.* **1965**, *42*, 3339−3340.
(22) Zeldes, H.; Livingston, R. *J. Chem. Phys.* **1966**, *45*, 1946−1954.
(23) Fessenden, R. W. *J. Phys. Chem.* **1967**, *71*, 74−83.
(24) Jackel, G. S.; Gordy, W. *Phys. Rev.* **1968**, *176*, 443−452.
(25) Fischer, H.; Hefter, H. *Z. Naturforsch. A* **1968**, *23*, 1763−1765.
(26) Riveros, J. M.; Shih, S. *J. Chem. Phys.* **1969**, *50*, 3132−3133.
(27) Greatorex, D.; Kemp, T. J. *J. Chem. Soc., Faraday Trans I* **1972**, *68*, 121−128.
(28) Hill, D. J. T.; O'Donnell, J. H.; Pomery, P. J.; Whittaker, A. K. *J. Photochem.* **1984**, *26*, 255−267.
(29) Cooley, L. F. Ph.D. Thesis, Brown University, 1987.
(30) Yamada, T.; Komaguchi, K.; Shiotani, M.; Benetis, N. P.; Sørnes, A. R. *J. Phys. Chem. A* **1999**, *103*, 4823−4829.
(31) Dmitriev Yu, A.; Zhitnikov, R. A. *J. Low Temp. Phys.* **2001**, *122*, 163−170.
(32) Dmitriev Yu, A.; Zhitnikov, R. A. *Low Temp. Phys.* **2003**, *29*, 519−521.
(33) Dmitriev Yu, A. *Physica B* **2004**, *352*, 383−389.

(34) Danilczuk, M.; Pogocki, D.; Lund, A.; Michalik, J. *J. Phys. Chem. B* **2006**, *110*, 24492−24497.
(35) Komaguchi, K.; Nomura, K.; Shiotani, M. *J. Phys. Chem. A* **2007**, *111*, 726−733.
(36) Popov, E.; Kiljunen, T.; Kunttu, H.; Eloranta, J. *J. Chem. Phys.* **2007**, *126*, 134504 (10 pages).
(37) Roduner, E. In *Isotope effects in chemistry and biology*; Kohen, A., Limbach, H.-H., Eds.; CRC Press: Boca Raton, FL, 2005.
(38) Walker, D. C. *Muon and Muonium Chemistry*; Cambridge University Press: Cambridge, U.K., 1983.
(39) Percival, P. W.; Brodovitch, J.-C.; Leung, S. K.; Yu, D.; Kiefl, R. F.; Luke, G. M.; Venkateswaran, K.; Cox, S. F. J. *Chem. Phys.* **1988**, *127*, 137−147.
(40) Yu, D.; Percival, P. W.; Brodovitch, J.-C.; Leung, S. K.; Kiefl, R. F.; Venkateswaran, K.; Cox, S. F. J. *Chem. Phys.* **1990**, *142*, 229−236.
(41) Roduner, E. *The Positive Muon as a Probe of Free Radical Chemistry*; Lecture Notes in Chemistry 49; Springer-Verlag: Berlin, 1988.
(42) Rhodes, C. J. *J. Chem. Soc., Perkins Trans 2* **2002**, 1379−1396.
(43) McKenzie, I.; Brodovitch, J.-C.; Ghandi, K.; Kecman, S.; Percival, P. W. *Physica B* **2003**, *326*, 76−80.
(44) McKenzie, I.; Brodovitch, J.-C.; Percival, P. W.; Ramnial, T.; Clyburne, J. A. C. *J. Am. Chem. Soc.* **2003**, *125*, 11565−11570.
(45) Addison-Jones, B. Ph.D. Thesis, Simon Fraser University, 2000.
(46) Addison-Jones, B.; Percival, P. W.; Brodovitch, J.-C.; Ji, F.; Sharma, D.; Wlodek, S. *Hyperfine Interact.* **1994**, *87*, 847−851.
(47) Addison-Jones, B.; Percival, P. W.; Brodovitch, J.-C.; Ji, F. *Hyperfine Interact.* **1997**, *106*, 143−149.
(48) McKenzie, I.; Addison-Jones, B.; Brodovitch, J.-C.; Ghandi, K.; Kecman, S.; Percival, P. W. *J. Phys. Chem. A* **2002**, *106*, 7083−7085.
(49) Bennett, J. E.; Mile, B. *J. Chem. Soc., Faraday Trans. 1* **1973**, *69*, 1398−1414.
(50) Improta, R.; Barone, V. *Chem. Rev.* **2004**, *104*, 1231−1253.
(51) Barone, V.; Minichino, C.; Faucher, H.; Subra, R.; Grand, A. *Chem. Phys. Lett.* **1993**, *205*, 324−330.
(52) Rega, N.; Cossi, M.; Barone, V. *J. Am. Chem. Soc.* **1997**, *119*, 12962−12967.
(53) Adamo, C.; Heitzmann, M.; Meilleur, F.; Rega, N.; Scalmani, G.; Grand, A.; Cadet, J.; Barone, V. *J. Am. Chem. Soc.* **2001**, *123*, 7113−7117.
(54) Vögel, A. I. *Vögel's Textbook of Practical Organic Chemistry*, 5th ed., revised by Furniss, B. S.; Longman: London, 1989, pp 100−102.
(55) Andreades, S.; Carlson, H. D. *Org. Synth., Collect. Vol. V* **1973**, 679−684.
(56) Fisher, G. J.; MacLean, A. F.; Schnizer, A. W. *J. Org. Chem.* **1953**, *18*, 1055−1057.
(57) Percival, P. W.; Addison-Jones, B.; Brodovitch, J.-C.; Ghandi, K.; Schüth, J. *Can. J. Chem.* **1999**, *77*, 326−331.
(58) Frisch, M. J.; et al. Gaussian 03, Revision B.04, Gaussian, Inc., Pittsburgh PA, 2003.
(59) Becke, A. D. *J. Chem. Phys.* **1993**, *98*, 1372−1377.
(60) McKenzie, I.; Addison-Jones, B.; Brodovitch, J.-C.; Ghandi, K.; Percival, P. W. *PhysChemComm* **2001**, *27*, 1−3.
(61) *NIST Computational Chemistry Comparison and Benchmark Database*; NIST Standard Reference Database No. 101, Release 12, Aug 2005; Johnson, R. D., III.; Ed.; http://srdata.nist.gov/cccbdb.
(62) McConnell, H. M.; Chesnut, D. B. *J. Chem. Phys.* **1958**, *28*, 107−117.
(63) Roduner, E.; Reid, I. D. *Isr. J. Chem.* **1989**, *29*, 3−11.
(64) Reddoch, A. H.; Konishi, S. *J. Chem. Phys.* **1979**, *70*, 2121−2130.
(65) Al-Bala'a, I.; Bates, Jr., R. D. *J. Magn. Reson.* **1987**, *73*, 78−89.
(66) Fernández, B.; Christiansen, O.; Bludsky, O.; Jørgensen, P.; Mikkelsen, K. V. *J. Chem. Phys.* **1996**, *104*, 629−635.
(67) Jursic, B. S. *Chem. Phys. Lett.* **1995**, *244*, 263−268.
(68) Wang, B.-Q.; Li, Z.-R.; Wu, D.; Hao, X.-Y.; Li, R.-J.; Sun, C.-C. *Chem. Phys. Lett.* **2003**, *375*, 91−95.
(69) Solimannejad, M.; Alikhani, M. E. *Chem. Phys. Lett.* **2005**, *406*, 351−354.
(70) Tachikawa, H. *J. Phys. Chem. A* **1998**, *102*, 7065−7069.
(71) Igarashi, M.; Ishibashi, T.; Tachikawa, H. *J. Mol. Struct.-THEOCHEM* **2002**, *594*, 61−69.
(72) Takada, T.; Tachikawa, H. *Int. J. Quantum Chem.* **2005**, *105*, 79−83.
(73) Stratt, R. M.; Desjardins, S. G. *J. Am. Chem. Soc.* **1984**, *106*, 256−257.
(74) Enthalpy of Vaporization. *CRC Handbook of Chemistry and Physics*, Internet Version 2007, 87th ed.; Lide; D. R., Ed.; Taylor and Francis: Boca Raton, FL, 2007.
(75) Yaws, C. L. *Chemical Properties Handbook*; McGraw-Hill: New York, 1999.